Available online at www.sciencedirect.com
ScienceDirect
Journal of the European Ceramic Society 29 (2009) 163–173
www.elsevier.com/locate/jeurceramsoc

Fabrication and characterization of fully dense Si–C–N ceramics from a poly(ureamethylvinyl)silazane precursor

Narayanan Janakiraman *, Fritz Aldinger

Max-Planck Institut für Metallforschung and Institut für Nichtmetallische Anorganische Materialien, Pulvermetallurgisches Laboratorium, Heisenbergstr. 3, D-70569 Stuttgart, Germany

Received 1 April 2008; received in revised form 26 May 2008; accepted 29 May 2008
Available online 7 July 2008

Abstract

Characterization of the intrinsic physical and mechanical properties of precursor-derived ceramics (PDC) is hitherto hindered by the unavailability of suitable specimens with the representative material structure, homogeneity and of sufficient dimensions amenable to the characterization method. The experimental response is often significantly modified by the included porosity and possible pseudo-microstructures, introduced through the sample fabrication. This paper describes the fabrication of fully dense homogeneous precursor-derived Si–C–N ceramic specimens with material structures covering amorphous to nano-crystalline state using a casting technique, from a liquid polysilazane precursor. The three critical problems involved in the dense PDC processing, viz., (i) bubble formation, (ii) gas evolution induced bloating and cracking and (iii) transformation induced cracking are addressed through controlled cross-linking and thermolysis techniques. Structural characterization of the specimens is carried out using FT-IR, Raman, XRD and HRTEM. The changes in the material structure in the amorphous and phase segregated state are correlated to the material properties, through preliminary physical and mechanical characterization.

Keywords: A. Precursors-organic; B. Nanocomposites; B. Spectroscopy; B. Electron microscopy; Si–C–N

1. Introduction

Polymer-derived silicon carbonitride (Si–C–N) ceramics are candidate materials for high temperature structural and functional applications in the form of fibers,[1–3] protective coatings,[4–6] fiber and particulate-reinforced composites[7] and since recently as components for micro-electro-mechanical devices (MEM).[8] The synthesis of these materials involves cross-linking and/or pyrolysis of suitable organo-silicon precursor polymers in an inert atmosphere, leading to ceramics with high purity, controlled structure and chemical composition.[9,10] Depending upon the chemistry of the starting precursor and pyrolysis conditions, a range of material structures from fully amorphous to nano-crystalline ceramics can be produced, with associated influence on the material properties. Knowledge of the intrinsic physical and mechanical properties of these materials is of interest, both from scientific and application perspectives.

Experimental evaluation of these properties, however, strongly relies on the availability of suitable samples that truly reflect the material behavior. Physical and mechanical characterization of these materials until now has been widely carried out[11–13] using monolithic samples fabricated through a powder consolidation route.[14,15] In this method, the cross-linked precursor powder with sufficient formability is warm-pressed under an optimized temperature–pressure program, yielding a green body with controlled porosity. The green body is in turn pyrolyzed at elevated temperatures to obtain a monolithic ceramic body albeit with residual porosity, invariably introduced to enable the escape of gaseous pyrolysis by-products. Also, the original particle boundaries of the starting powder can be still retained to varying extents depending on the conditions of warm pressing and/or reactivity of the powder, leading to a pseudo-microstructure in an otherwise amorphous sample. Such features can adversely affect the evaluation of properties relating to fracture (through crack deflection along boundaries, arrest at pores, etc.), and can significantly modify other properties, depending

* Corresponding author. Present address: Institut für Nichtmetallische Werkstoffe, Technische Universität Clausthal, Zehntnerstr. 2a, 38678 Clausthal-Zellerfeld, Germany. Tel.: +49 5323 72 3537; fax: +49 5323 72 3710.
E-mail address: nja@tu-clausthal.de (N. Janakiraman).

0955-2219/$ – see front matter © 2008 Elsevier Ltd. All rights reserved.
doi:10.1016/j.jeurceramsoc.2008.05.028

upon the extent, shape and distribution of such features and their interaction with the experimental conditions. Several hybrid methods have been described in literature to improve the bulk density of the powder-derived ceramic bodies with varying success or applicability.[16–18] However, for the characterization of the intrinsic mechanical properties of precursor-derived ceramics (PDC), fully dense bulk specimens of sufficient size and free of processing-generated pseudo-microstructure are necessary. A promising strategy is to fabricate fully dense monolithic infusible green bodies free of processing-generated microstructure from suitable precursors, and a direct polymer to ceramic transformation of these green bodies using controlled pyrolysis. Depending upon the rheology, melting and cross-linking characteristics of the candidate precursor, the first step can be realized using either a warm consolidation – cross-linking or a casting – cross-linking procedure.[19,20] The latter route is ideally suitable for cross-linkable liquid precursors.

The major difficulties with the fabrication of fully dense monolithic ceramics from liquid precursors are:[17,21,22]

(i) Bubble formation/foaming during thermal cross-linking.
(ii) Restriction of degassing during pyrolysis.
(iii) Material shrinkage.

Bubble formation can occur due to the evaporation of the liquid precursor, the extent of which is determined by the cross-linking temperature, heating rate, ambient pressure and polymer viscosity. A coupled increase of bulk density and the volume to surface ratio of the cross-linked green body restricts the removal of gaseous by-products released during pyrolysis reactions. This increases the pressure within the bulk of the body resulting in bloating and/or cracking. The above, as well as any possible temperature gradient across the bulk can lead to a differential rate of polymer to ceramic transformation from surface to the core of the specimen, thereby, a differential shrinkage. This eventually results in cracking or complete disintegration of the pyrolyzed body. Considerable research has been carried out in the mathematical handling of the above problems.[23–25] However, reports on the successful fabrication of dense monolithic ceramics from polymer precursors are limited. Freimuth et al. have reported the fabrication of miniaturized ceramic structures through the pyrolysis of green forms obtained using a solution casting process.[19] The polymer forms were chemically cross-linked in air and the pyrolysis was conducted using extremely low heating rates ($\leq$10 K/h) to realize crack-free structures with a thickness of the order of several micrometers. Shah and Raj have recently developed a pressure casting technique[20] that enables fabrication of amorphous Si–C–N ceramic specimens with a thickness of $\leq$0.5 mm. In a comparable work, Sorarù et al. have successfully fabricated fully dense Si–C–O glasses in the form of thin rods ($\sim$1.5 mm diameter; 30 mm long) suitable for mechanical characterization, using a gel-casting technique.[26]

In this work we report an improved method for the fabrication of fully dense defect free ceramic bodies from a liquid poly(ureamethylvinyl)silazane (PUMVS) precursor, that are suitable for a range of physical and mechanical characterization experiments. While the methodology closely follows the work of Shah and Raj,[20] capabilities with respect to the obtainable specimen thickness and material structures have been enhanced, and the need for employing a pressure vessel is eliminated. Additionally, the structural, physical and mechanical characterization of these specimens covering partly organic to nano-crystalline Si–C–N ceramics are presented.

2. Experimental procedure

The liquid precursor PUMVS, commercially known as Ceraset® (KiON Corporation, Columbus, OH) was cast into a PTFE mould, hermetically sealed in a steel die and thermally cross-linked at 260 °C for 5 h to form fully dense, transparent infusible green bodies. A schematic diagram of the mould-die construction is shown in Fig. 1. The PTFE mould was made out of three circular PTFE discs of 1 mm thickness, the middle disc having a circular recess. The bottom and middle discs were glued together to form the mould cavity, using a thin layer of two-component epoxy glue. The liquid precursor was filled into the mould cavity, closed with the third disc, sandwiched together between the two halves of the steel die and tightened with screws. PTFE was chosen as mould material due to its easy formability and mould releasing characteristics. The die was placed in a quartz glass with Schlenk construction, which was evacuated and back-filled with nitrogen. The entire assembly was then placed in a furnace and heated to 360 °C using a programmable furnace controller. A higher furnace temperature was necessary to realize the actual cross-linking temperature of 260 °C at the cross-linking die, which was monitored using a second thermocouple. The cross-linked green bodies were disc shaped, with a diameter of 19 mm and 1 mm thickness.

The mass loss and shrinkage behavior of the green bodies during pyrolysis were determined by thermo-gravimetric analysis (TGA) and thermo-mechanical (TMA) analysis, respectively (RT $\leq T_p \leq$ 1000 °C; heating rate: 5 K/min; atmosphere: flowing argon). A cross-linked sample with a thickness of 1 mm was used for the TMA. The analyses were performed using a simultaneous thermal analyzer (model STA-409 Netsch) for TG and a thermo-mechanical analyzer (model TMA2000, Bähr thermoanalyse, Hillhorst, Germany) for TMA.

Several batches of green bodies were pyrolyzed in a flowing inert gas atmosphere using Schlenk tubes to various final temperatures (T_p) from 800 to 1500 °C in steps of 100 °C to obtain ceramic samples with a range of material structures. For samples

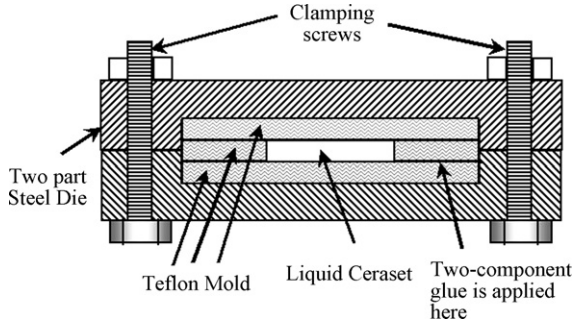

Fig. 1. Schematic diagram of the mold-die construction.

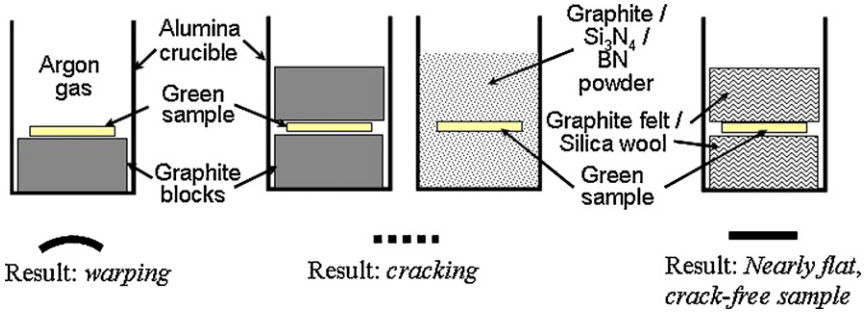

Fig. 2. Schematic illustration of the methods experimented using different heat transfer media and sample placement during pyrolysis for realizing crack-free dense Si–C–N ceramic specimens.

pyrolyzed up to 1000 °C, a single stage pyrolysis schedule was employed (800 °C ≤ T_p ≤ 1000 °C; heating rate: 100 K/h; hold time at T_p: 1 h; cooling rate: 300 K/h; atmosphere: flowing argon; Schlenk tube: quartz). An additional heating ramp was included in the heating schedule for samples pyrolyzed at 1100 °C, at 10 K/h from 1000 to 1100 °C. In order to control the temperature distribution and thereby the heat transfer to the green bodies during pyrolysis, several trials were carried out by changing the heat transfer media and sample placement. These methods are schematically illustrated in Fig. 2 and included: (i) sandwiching the green bodies between or simply placing them on monolithic graphite blocks; (ii) powder bed method, where the green bodies were packed in loose Si_3N_4, BN or graphite powder; (iii) packing the green bodies within silica wool; (iv) sandwiching between porous graphite felt. The green samples along with the heat transfer media were packed within an alumina crucible, which was then placed in the Schlenk tube. As will be described in Section 3.1, the arrangement with graphite felt was successfully used for the preparation of Si–C–N ceramics up to a pyrolysis temperature of 1100 °C. A two-stage pyrolysis–annealing schedule was used for samples above 1100 °C. In this case, Si–C–N ceramic samples were pyrolyzed at T_p = 1000 °C in the first stage using the above method. In the second stage, these samples were mechanically ground and polished to remove surface defects, packed in boron nitride (BN) powder inside an alumina crucible and subjected to a second annealing treatment (heating rate: 100 K/h for RT < T < 1000 °C; 10 K/h for 1000 °C < T ≤ 1500 °C; holding time at T_p: 12 h; cooling rate: 300 K/h; atmosphere: flowing nitrogen; Schlenk tube: alumina). In the following, the samples will be referred according to their thermal treatment, e.g., SiCN-080001, SiCN-090001, SiCN-100001, SiCN-110001, SiCN-120012, SiCN-130012 and SiCN-150012, the first four digits denoting the temperature and the last two digits, the holding time of the pyrolysis or annealing treatment in hours.

Structural characterization of the samples was performed using FT-IR, Raman spectroscopy, X-ray diffraction (XRD) and high-resolution transmission electron microscopy (HRTEM). Infrared spectra were collected in transmission using KBr pellets (Nicolet spectrometer, Model Magna 560) in the wave number range 4000–450 cm^{-1} and a spectral resolution of 4 cm^{-1}. Raman spectroscopy was carried out using a Jobin Yvon spectrometer (excitation source: He–Ne laser, λ = 632.8 nm; laser power: 0.004–0.4 mW; sample objective: 20X/50X; spectral resolution: 4 cm^{-1}). For XRD analysis, a Siemens diffractometer (Model D5000 Kristalloflex; Cu Kα radiation, λ = 1.5406 Å) was employed. HRTEM was performed using a Philips CM200 (Philips Eindhoven, Netherlands) instrument. TEM samples were prepared according to the standard procedure, involving drilling, grinding, dimpling and finally ion-milling. In addition, light microscopy and scanning electron microscopy (SEM, Cambridge instruments S200 as well as FESEM, Gemini DSM 982 and JEOL JSM 6300F) were utilized to examine polished as well as fracture surfaces of samples. Bulk chemical analyses were performed by atomic emission spectroscopy with inductively coupled plasma excitation (for silicon), combustion (for carbon and hydrogen) and carrier gas hot extraction (for nitrogen and oxygen).

Density of the samples was measured by Archimedes method in water for monolithic samples, as well as by helium pycnometry (Micromeritics, Model Accupyc1330) for powdered samples. Young's modulus and poisons ratio were determined by the resonance frequency analysis method (RFDA, IMCE n.v., Dipenbeek, Belgium) using circular disc specimens with a diameter of 12 mm and a nominal thickness of 300 μm. The method involves the analysis of the resonance frequencies generated from the mechanical excitation of the specimen, which is then related to the specimen geometry, density and elastic modulus. Hardness of the samples was evaluated using Vickers diamond pyramid indentation under various loads, viz., 0.245, 0.490, 0.981, 1.962, 4.905, 9.81, 19.62 and 49.05 N. Thermal diffusivity of the samples was determined by the laser flash method, using circular disc specimens as above.

3. Results

3.1. Fabrication of fully dense samples

A temperature–time combination of 260 °C–5 h was found to be optimum for the cross-linking of the liquid PUMVS precursor to yield hard, fully dense and transparent green bodies (Fig. 3). While the use of higher temperatures initiated the deformation of PTFE mould, use of lower temperatures or holding times resulted in insufficient cross-linking, producing rubber-like bodies.

The pyrolysis of green bodies was found to be the critical step in the fabrication of dense ceramic specimens. Pyrolysis of dense green bodies with thickness higher than 2 mm always resulted in

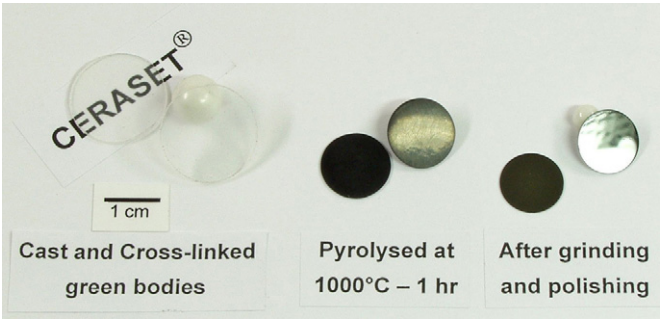

Fig. 3. Typical fully dense samples at various processing conditions. The pyrolyzed and polished samples display, respectively, diffuse and specular reflection of light.

bloating (Fig. 4) accompanied by severe cracking. Samples with thickness ≤1 mm did not show bloating; however, mild to extensive cracking was observed. Light microscopy of cross-sections of the fragments themselves confirmed the absence of bloating, gas bubbles or porosity, within the resolution of the technique. Severity of cracking appeared to be reduced by reducing sample thickness below 1 mm, but was not eliminated. Up to a pyrolysis temperature of 1000 °C, cracking was not affected by surface finish or any other stress raising features in the green bodies. Also, in the same temperature range, heating rate did not have a significant influence on the above results. To elaborate, cracking occurred even with a heating rate as low as 5 K/h.

In order to control the heat transfer to the samples during pyrolysis, different arrangements with respect to the sample placement were tried (Fig. 2). When placed on a flat graphite block with the top surface open to the atmosphere, samples showed warping into a dish shape, concave downwards, with little or no cracking. Thinner samples favored warping to cracking than thicker samples, where warping and cracking were inversely related. Pyrolysis of samples sandwiched between two graphite blocks always led to complete cracking. Use of powder bed techniques with graphite, Si_3N_4 or BN powders also could not avert cracking during the pyrolysis of green bodies. However, interestingly, when wrapped in silica wool, they could

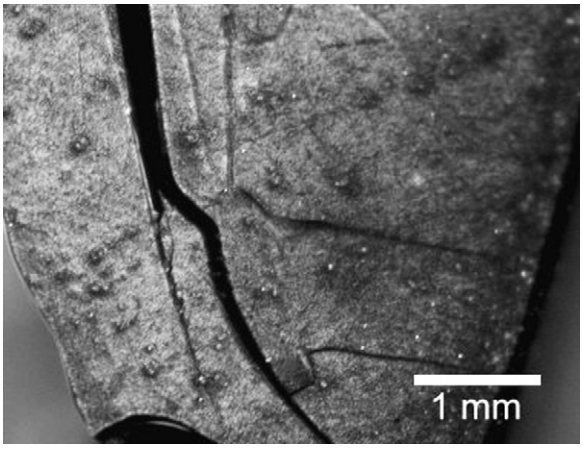

Fig. 4. Light micrograph of a sample pyrolyzed at 1000 °C–1 h, from a fully dense green body with a starting thickness of 2 mm; blisters due to bloating and severe cracking are evident.

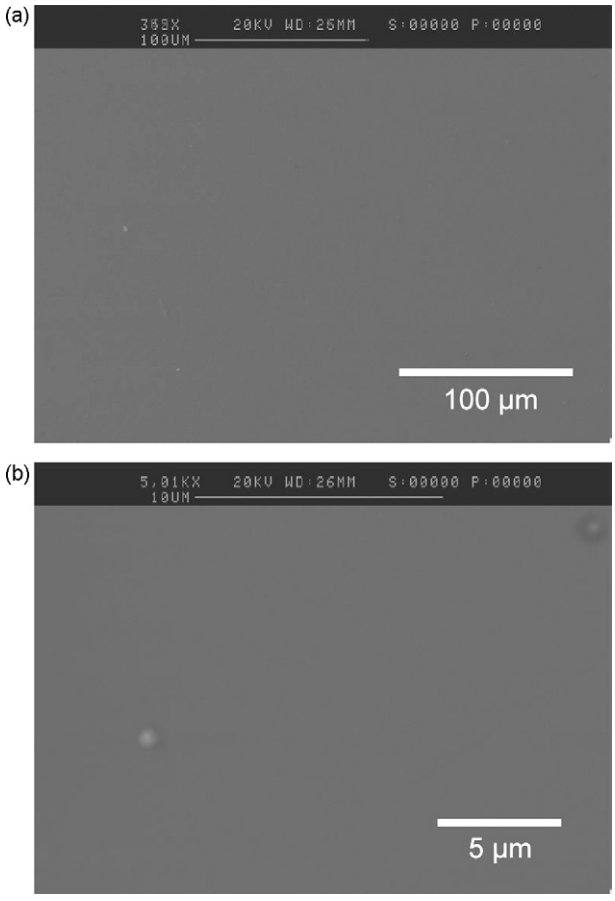

Fig. 5. SEM micrographs from the polished surface of the SiCN-110001 sample corroborating the dense pore-free structure.

be pyrolyzed free of cracks with only mild warping, which was concentrated in regions where packing density of silica wool was high. Taking lead from this, the dense green bodies were pyrolyzed as sandwiched between two porous graphite felts. This yielded dense ceramic bodies free of cracks and with minimal warping up to 1000 °C, in spite of the relatively high heating rate of 100 K/h employed. Note that this heating rate is higher by a factor of 4–10 times than those employed by Shah and Raj and Freimuth et al.[19,20] For samples pyrolyzed at 1100 °C, a reduction of heating rate to 10 K/h was necessary above 1000 °C to avert cracking. A photograph of typical samples before and after pyrolysis is given in Fig. 3. SEM micrographs (Fig. 5) of the SiCN-110001 sample at two different magnifications substantiate the dense structure of the material.

For the preparation of homogeneous Si–C–N ceramic samples subjected to thermal treatment above 1100 °C, use of graphite felt as heat transfer medium was found unsuitable. This was due to the chemical interaction between Si–C–N sample and graphite felt in contact resulting in accelerated crystallization at and near the sample surface, producing a layered microstructure across the sample thickness. Cracks initiated and propagated from stress raising features (such as surface and edge roughness), particularly favored by the accumulated residual stresses during pyrolysis. To counter the above, two modifications were applied for samples prepared at T_p above 1000 °C. A two-

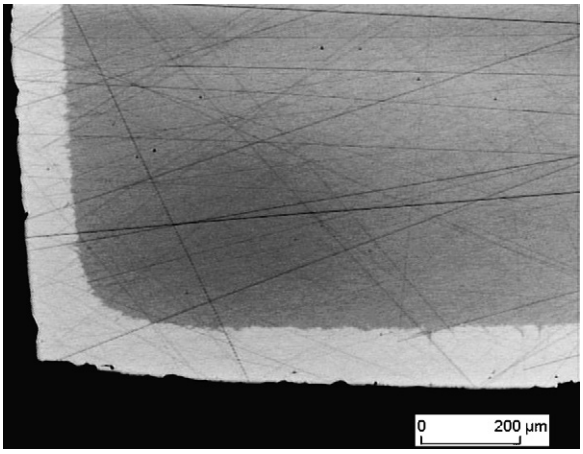

Fig. 6. Polished cross-section of the SiCN-130012 sample.

stage pyrolysis–annealing sequence was adopted as described in Section 2, with an intermediate grinding and polishing procedure applied to relieve the accumulated residual stresses and to remove the surface defects. The active chemical reactions with the pyrolysis environment such as the above were obviated by the use of a BN powder bed (which is chemically inert to Si–C–N ceramics at the employed temperatures) and a flowing nitrogen gas atmosphere. This procedure yielded fully dense crack-free samples with an acceptable homogeneous microstructure up to an annealing treatment at 1300 °C/12 h, where the affected layer thickness was 50–100 μm from the sample surface (Fig. 6). Heterogeneous features appeared across the sample cross-section at annealing temperatures above 1400 °C, and are evident from the fractured as well as polished cross-sections of SiCN-150012 sample (Fig. 7). A layered microstructure near the surfaces, accompanied by globular features spreading along the middle plane of the sample thickness is observed (Fig. 7a). A crack introduced in this region through Vickers indentation propagated across as well as around these globular features (light micrograph, (Fig. 7b). That the fracture occurred through as well as around the globules is discerned from the SEM fractograph at higher magnification (Fig. 7c), where the globular features appear as flat, concave as well as convex surfaces, suggesting that these features were not closed pores, but dense material separated from the matrix along a weak interface. Although free from porosity, these samples cannot be used for physical and mechanical characterization, as the microstructure is not homogeneous across the cross-section.

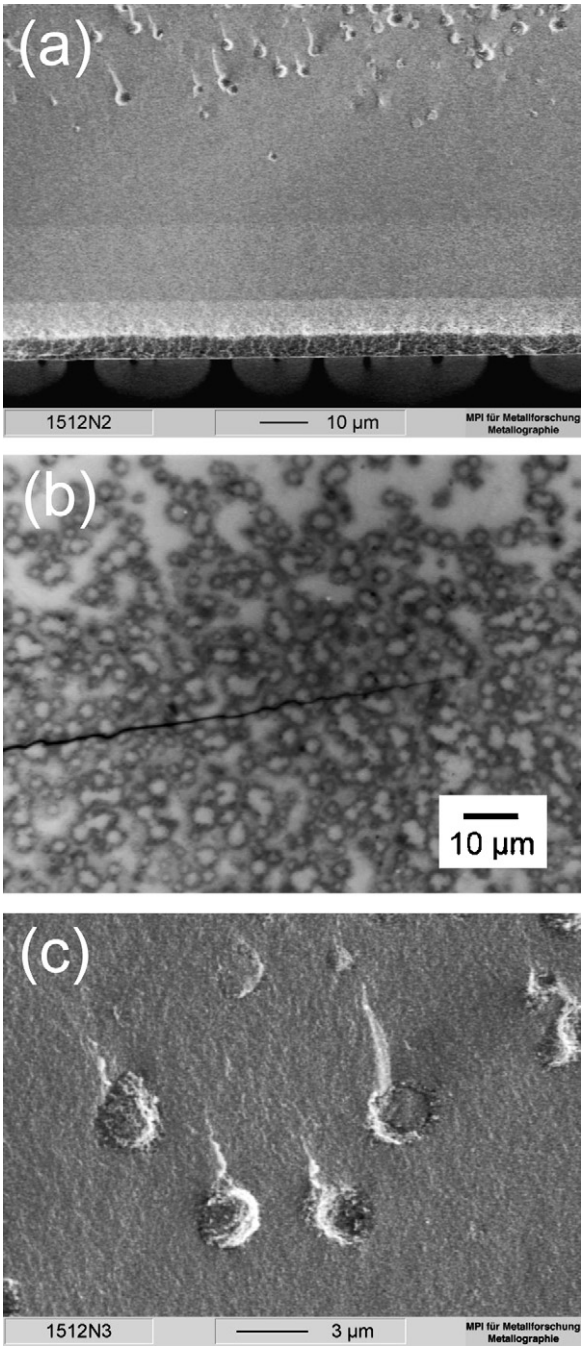

Fig. 7. Fractured as well as polished cross-sections of the SiCN-150012 sample: (a) and (c) SEM fractographs; (b) light micrograph of the polished cross-section, containing a Vickers indentation crack.

3.2. Chemical and structural characterization

3.2.1. Bulk chemical analysis

The elemental compositions and the empirical formulas of the thermolyzed samples at different temperatures from 800 to 1300 °C are given in Table 1. Interestingly, the analyses showed almost no variation in silicon, carbon and nitrogen content. However, the samples pyrolyzed at lower temperatures contained appreciable quantities of hydrogen. The hydrogen content decreased continuously with increasing thermal treatment, falling below the detection limits in SiCN-120012 and SiCN-130012. Considerable oxygen contamination was also present in the samples, resulting from the handling of green bodies in air. Assuming that the silicon atoms bond to oxygen, nitrogen and carbon atoms corresponding to equivalent stoichiometric quantities of SiO_2, Si_3N_4 and SiC, the amount of 'free carbon' in the material can be calculated for SiCN-120012 and SiCN-130012 from their empirical formulas and are given as $SiC_{0.33}N_{0.77}O_{0.18} + 0.62\ C_{free}$ and $SiC_{0.36}N_{0.76}O_{0.14} + 0.54\ C_{free}$, respectively.

Table 1
Elemental composition of the specimens as a function of pyrolysis temperature, determined from bulk chemical analysis

Sample	Elemental composition										Empirical formula
	Si		C		N		H		O		
	(wt%)	(at.%)	(wt%)	(at.%)	(wt%)	(at.%)	(wt%)	(at.%)	(wt%)	(at.%)	
SiCN-080001	52.6	25.86	22.4	25.75	20.6	20.3	1.9	26.02	2.4	2.07	$SiCN_{0.78}O_{0.08}H$
SiCN-090001	52.7	27.33	22.2	26.92	22.2	23.09	1.48	21.39	1.4	1.27	$SiC_{0.98}N_{0.84}O_{0.05}H_{0.78}$
SiCN-100001	53	29.56	22.7	29.6	21.2	23.71	0.97	15.07	2.1	2.06	$SiCN_{0.80}O_{0.07}H_{0.51}$
SiCN-110001	54	31.31	22.1	29.96	21.5	24.99	0.75	12.12	1.6	1.63	$SiC_{0.96}N_{0.80}O_{0.05}H_{0.39}$
SiCN-120012	52.5	33.85	21.4	32.26	20.1	25.98	<0.1	<1.8	5.4	6.11	$SiC_{0.95}N_{0.77}O_{0.18}$
SiCN-130012	54.7	35.45	21.1	31.98	20.6	26.77	<0.1	<1.8	4.3	4.89	$SiC_{0.90}N_{0.76}O_{0.14}$

3.2.2. FT-IR

The transmission FT-IR spectra (Fig. 8) depict the structural changes in the samples with increasing thermal treatment. The spectrum from SiCN-080001 sample shows a broad composite absorption band of higher relative intensity in the range 800–1100 cm^{-1} as well as lower intensity bands at 2129, 1403, and 1255 cm^{-1} (as a shoulder). The composite band comprises of superposed Si–N (910, 985, and 1040 cm^{-1})[27] and Si–C (780 and 900 cm^{-1})[28] bond vibrations, while the low intensity bands arise from Si–H, C–H, and Si–CH_3 vibrations, respectively.[10] With increasing pyrolysis temperature, the Si–H, C–H, and Si–CH_3 bands decreased in intensity further, and were undetectable in the SiCN-110001 sample. A simultaneous increase in the intensity of the Si–C bands relative to the Si–N bands was observed, evident from the change of shape of the composite peak. The features located around 1610 cm^{-1} are attributable to the oxygen or moisture contamination during handling of the samples in air.

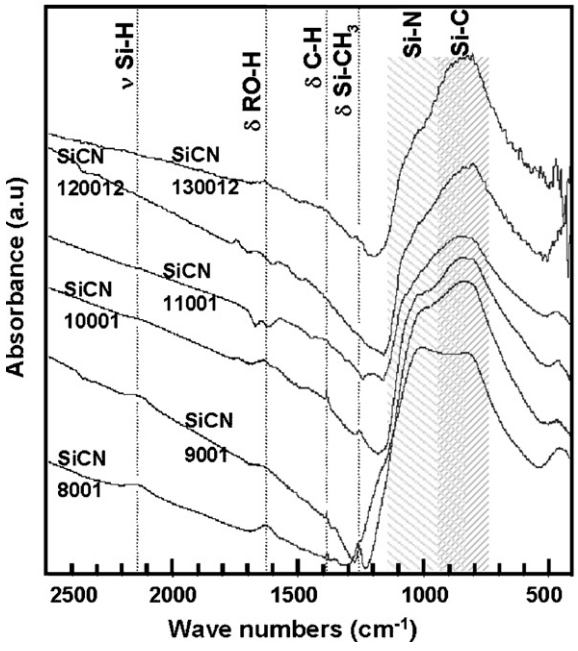

Fig. 8. Transmission FT-IR spectra of Si–C–N samples pyrolyzed or annealed at various temperatures between 800 and 1300 °C.

3.2.3. Raman spectroscopy

Fig. 9a shows the Raman spectra recorded from the samples pyrolyzed at different temperatures. The overall relative intensities of the spectra progressively decreased with increasing pyrolysis temperature. The presented spectra are therefore suitably rescaled for better clarity. The spectrum from the SiCN-080001 sample displayed no phonon modes but only a large background signal. While the background intensity was still

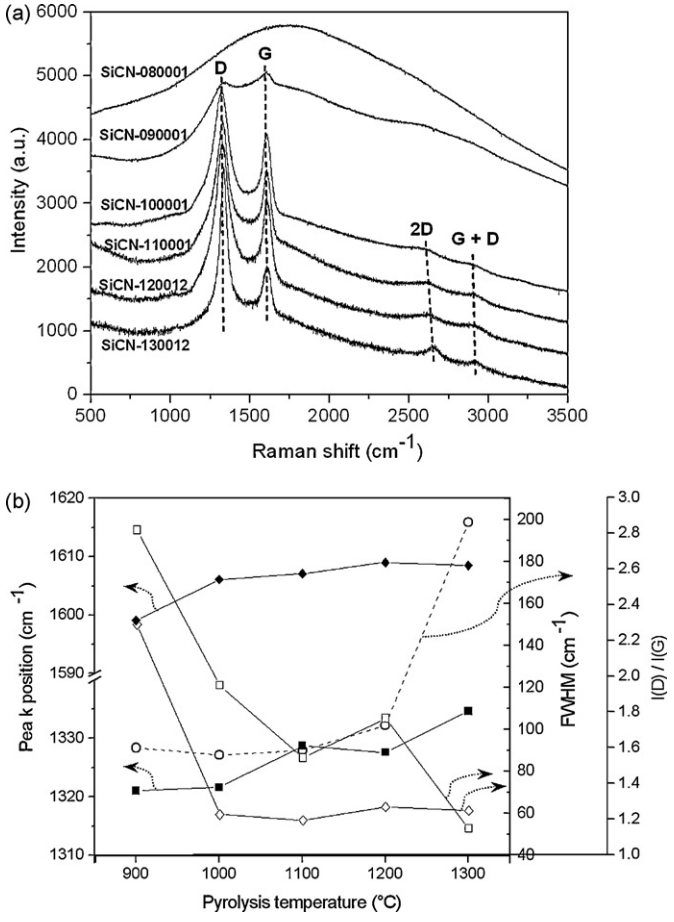

Fig. 9. Raman analysis of Si–C–N samples pyrolyzed or annealed at various temperatures between 800 and 1300 °C: (a) Raman spectra showing the evolution of D and G peaks (b) variation of D and G peak positions, FWHM and the intensity ratio $I(D)/I(G)$ with thermal treatment; square and diamond symbols (open as well as filled) indicate D and G peaks, respectively.

appreciable in the spectrum of the SiCN-090001 sample, two peaks centered around 1320 and 1600 cm^{-1} were discernable, that correspond to the D and G peaks observed in disordered carbons.[29,30] The G peak arises from the stretching mode (E_{2g}) of the sp^2 C–C bonds, whereas the D peak originates from the breathing mode (A_{1g}) of the sp^2 rings.[30] The background signal in these spectra is due to the strong photoluminescence, which characterizes the polymeric nature of these samples containing appreciable quantities of hydrogen.[30,31] In the spectra of samples from higher thermal treatment, the D and G peaks were better resolved against a lower background. Additionally, new peaks appeared centered at around 2620, 2920, and 3230 cm^{-1} and are attributed to the overtones or combinations of the above mentioned first order phonon modes.[32,33] In order to appreciate the structural changes in the samples with increasing thermal treatment, a multiple peak curve fitting procedure using four Lorentzians (one each for the D and G peaks and the remaining two to account for the features around ~1200 and ~1500 cm^{-1}) was applied to the spectra to extract information, viz., peak position, peak width (full width at half maximum, FWHM), and relative intensity. The data are plotted in Fig. 9b. With increasing pyrolysis temperature the D peak showed a small but continuous upward shift in position and a steady decrease of its peak width ($FWHM_D$). Also, a simultaneous increase of its relative intensity I(D) compared with that of the G peak (I(G)) was observed, quantified as the net increase in the intensity ratio $I(D)/I(G)$. In contrast, the G peak position and width ($FWHM_G$) stabilized at 1000 °C and showed negligible variation above this temperature.

The population of all C–C bonds and the distribution of the C–C bond angle determine the intensity and the width of the G peak, respectively. The presence of G peak in the spectrum from SiCN-090001 signifies the early inception of disordered sp^2 carbon clusters in the material. This combined with the presence of D peak indicates that at least a significant fraction of carbon atoms are bonded as ring-like configurations. The D peak shift, peak width and intensity are correlated to the distribution of cluster size and order of carbon atoms. An increase in the number of ordered sixfold aromatic rings shifts the D peak upwards and increases its intensity, while the presence of *non-aromatic* disordered ring-like configurations increases the peak width at the cost of intensity.[31] The increase of the intensity ratio $I(D)/I(G)$ and the decrease of the D peak width thus correspond to the increase in the ordering of the clusters into aromatic graphene layers. The above results in total indicate the segregation, ordering and growth of carbon clusters towards the formation of nano-crystalline graphitic regions, in samples from higher thermal treatment.

3.2.4. X-ray diffraction

The results of the XRD measurements are compiled in Fig. 10. XRD patterns of the samples pyrolyzed up to 1100 °C showed no diffraction lines, but only broad diffraction humps, typical of amorphous materials. XRD pattern from SiCN-120012 sample showed a single broad peak centered at $2\theta = 36°$. The intensity and sharpness of this peak increased in the SiCN-130012 sample, along with the appearance of two broad peaks centered at $2\theta = 61°$ and 72°, respectively. Together, these three peaks indicate the nucleation of α/β-SiC. Additionally, a broad feature in the 2θ range between 21° and 30° was observed. Referring to the phase analysis of similar precursor-derived ceramics,[28,34] this can be attributed to the formation of the turbostratic carbon phase ($2\theta_{(200)\text{-Graphite}} = 26.592°$). Strong diffraction peaks corresponding to α-Si_3N_4 and α-SiC were observed in the SiCN-150012 sample, indicating appreciable crystallization at this annealing temperature.

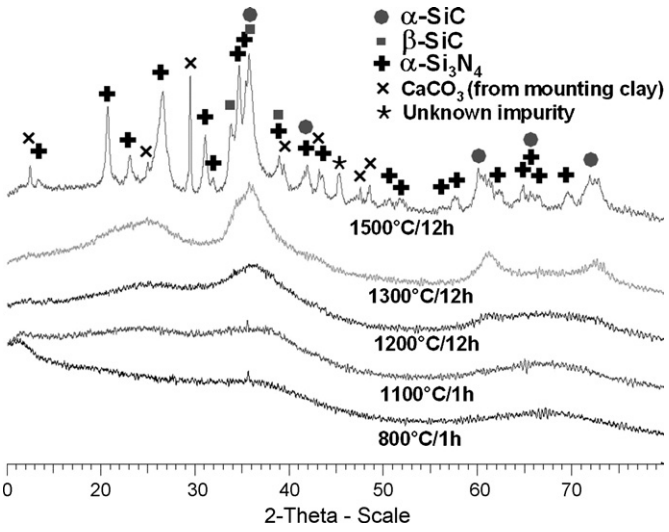

Fig. 10. X-ray diffraction patterns of Si–C–N samples pyrolyzed or annealed at various temperatures between 800 and 1500 °C.

3.2.5. High-resolution transmission electron microscopy

Microstructural evolution in samples treated at higher temperatures were analyzed using transmission electron microscopy under high-resolution. Accordingly, the high-resolution images along with the selected area electron diffraction (SAED) patterns from SiCN-110001, SiCN-120012 and SiCN-130012 samples were obtained and are presented in Fig. 11. The SAED patterns from SiCN-110001 and SiCN-120012 showed only diffuse halos typical of amorphous materials. TEM examination of the samples pyrolyzed below 1100 °C (e.g., SiCN-100001) using SAED and high resolution imaging revealed no structural features resolvable by electron diffraction and as such these materials can be classified as 'electron-amorphous'.[35] However, the high-resolution image from the SiCN-110001 sample contained regions of tiny layer-like curved features. The insets within the main image depict enlarged views of the regions of interest for clarity (Fig. 11a). While the morphology of these features is not readily discriminable from the surrounding matrix, comparison of similar features in higher temperature treated samples indicates that these are indeed precursors to the nano-scale clustering of the turbostratic graphite phase.[35–37] This is evidenced from the HR image of the SiCN-120012 sample (Fig. 11b). The turbostratic phase (marked 'B' in the insets) in the latter sample displayed improved ordering than the former, with the size ranging between 5 and 10 nm along the layers. The organization and size further improved in the SiCN-130012 sample in direc-

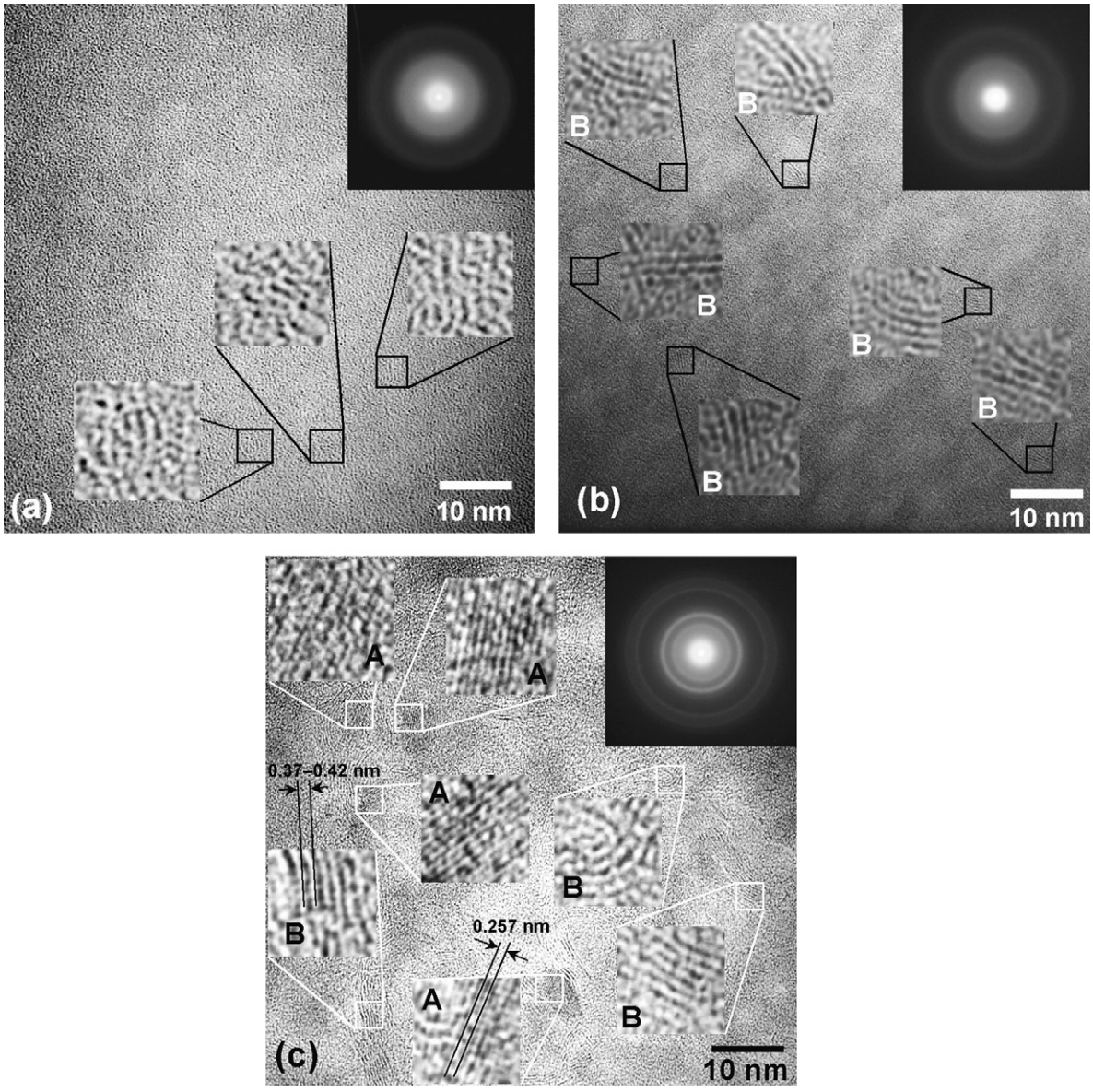

Fig. 11. HRTEM analysis of samples subjected to higher thermal treatment: (a) SiCN-110001, (b) SiCN-120012 and (c) SiCN-130012. The SAED patterns of the representative regions are also included as insets. Additional insets show enlarged views of the details of interest: A—SiC nano-crystals; B—turbostratic graphitic clusters.

tions along as well as perpendicular to the graphitic planes by stacking of several layers. The typical dimensions of the layers ranged from 15 to 30 nm along the layers consisting of seven to eight layers in a stack.[35] The inter-layer spacing, however, was appreciably different from that of crystalline graphite, and varies between 0.37 and 0.42 nm. Concurrent to the growth and ordering of the turbostratic graphitic phase, nucleation of nano-crystalline silicon carbide was observed in the SiCN-130012 sample.[35] The SAED pattern from this sample (Fig. 11c) shows three high relative intensity diffraction rings at ~4, ~6.5, and ~7.5 nm^{-1} corresponding to the $(1\,1\,1)_{\beta\text{-SiC}}$, $(2\,2\,0)_{\beta\text{-SiC}}$ and $(3\,1\,1)_{\beta\text{-SiC}}$ planes. The insets show high-resolution images of typical nano-crystallites (marked 'A'). The inter-planar spacing was measured to be 0.257 nm, which corresponds to the *d*-spacing of the $(1\,1\,1)_{SiC}$ planes.

3.3. Physical and mechanical characterization

The density, hardness and elastic constants of the investigated materials are summarized in Table 2. The density of the fully dense green bodies was 1.1 g/cm^3. With increasing pyrolysis treatment, the density monotonically increased from 1.85 g/cm^3 for SiCN-080001 sample to 2.15 g/cm^3 for the SiCN-120012 and SiCN-130012 sample, indicating the densification of the material structure. The Young's modulus determined from the resonance frequency method increased with thermal treatment to a maximum of 140 GPa in SiCN-120012 sample, above which it dropped to 117 GPa in SiCN-130012 sample. In contrast, Vickers hardness was found to have a maximum in SiCN-100001 sample at 11.3 GPa. This variation in the elastic and plastic response of the material is further discussed in the next section.

Table 2
Physical and mechanical properties of the pyrolyzed specimens as a function of the temperature of pyrolysis

Sample	Density (g/cm^3)	Young's modulus (GPa)	Poisson's ratio	Hardness (GPa)	Thermal diffusivity, $\times 10^{-7}$ (m^2/s)
SiCN-080001	1.85 ± 0.02	82 ± 1	0.245 ± 0.015	8.3 ± 0.1	5.07 ± 0.31
SiCN-090001	1.90 ± 0.02	106 ± 1	0.24 ± 0.005	9.5 ± 0.3	4.95 ± 0.07
SiCN-100001	2.00 ± 0.02	117 ± 1	0.22 ± 0.003	11.3 ± 0.4	4.14 ± 0.24
SiCN-110001	2.10 ± 0.02	127 ± 1	0.21 ± 0.005	9.7 ± 0.4	3.99 ± 0.23
SiCN-120012	2.16 ± 0.02	140 ± 4	0.22 ± 0.01	9.6 ± 0.3	5.50 ± 0.27
SiCN-130012	2.15 ± 0.02	117 ± 4	0.23 ± 0.01	7.9 ± 0.2	8.08 ± 0.16

4. Discussion

Cross-linking of the liquid precursor by heating without pressure leads to the formation of gas bubbles in the green body, due the evaporation of low molecular weight oligomers, dissolved gases and/or dissociation of weakly attached end groups. This is obviated in the present method by heating the precursor confined in a steel die, where the generated internal isostatic pressure eliminates bubble formation and yields fully dense glassy green bodies. Extensive gas evolution[38] and coupled mass loss occurs during pyrolysis of green bodies in the temperature window of 400–800 °C (Fig. 12). Restriction of the gas evolution in thicker samples (>1.5 mm) leads to bloating near the free surface and pressure build up in the sample core. Extensive bloating has been observed previously in the pyrolysis of powder-derived green bodies containing a higher fraction of closed pores, resulting from the higher warm pressing temperatures employed.[39] The relatively softer material at the initial stage of pyrolysis accommodates the stresses by deformation.[15,17] However, the progressing ceramization at higher pyrolysis temperatures renders the material stiff, leading to the cracking of the bodies. Limiting the green body thickness to 1 mm eliminates the gas pressure induced stresses. In this case, the diffusion through the relatively open structure of the green body sufficiently allows the escape of gaseous pyrolytic products. A more critical problem is the differential rate of polymer to ceramic transformation across the sample thickness, mainly arising from the differential heat transfer at the surface and the core regions. In the experiments, samples pyrolyzed as sandwiched between graphite blocks or packed in a powder bed were always cracked, whereas those pyrolyzed as simply supported on a single graphite block were warped. The relatively higher thermal conductivity of these heat transfer media in contact with the sample, in combination with the poor thermal conductivity of the sample, induces significant thermal gradients across the sample thickness. The consequent differential ceramization and the differential pyrolytic shrinkage produce transformation stresses, leading to cracking or warping of the samples. The porous graphite felt used as sample support and heat transfer medium in the present work possesses a low thermal conductivity, and thus effectively moderates the conductive heat transfer to the samples, reducing the thermal gradients to tolerable levels, while the porosity facilitates the escape of pyrolytic gases. The resulting ceramic bodies are dense and crack-free up to a pyrolysis temperature of 1100 °C, albeit containing considerable residual stresses. The intermediate machining of the amorphous samples, in addition to the removal of surface defects and chemical contamination, serves to relieve these stresses, enabling the successful fabrication of phase segregated samples through the second stage annealing treatment. Removal of residual stresses is also a prerequisite for the meaningful mechanical characterization of these materials.

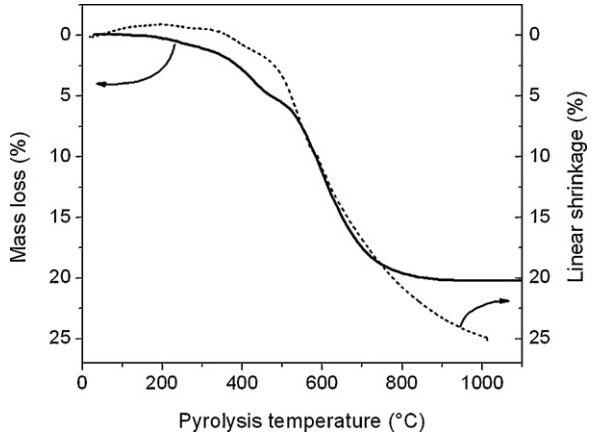

Fig. 12. Mass loss and linear shrinkage behavior during the pyrolysis of the cross-linked Si–C–N green bodies, recorded from TG and TMA analyses, respectively.

A detailed account of the polymer to ceramic transformation of the PUMVS precursor has been described by Li et al.[38] The chemical and structural characterization presented here highlights the change in the material structure of the fully dense Si–C–N–(H) ceramic specimens thermolyzed from the above precursor to varying degrees of conversion, such that a correlation to the physical and mechanical behavior can be examined. The chemical composition of the all the thermolyzed specimens remains nearly invariant, barring hydrogen content. This is due to the completion of the majority of the pyrolytic reactions by 800 °C, as revealed by the TG (Fig. 12) and TG coupled mass spectrometry.[38] The materials from thermolysis treatments up to 1000 °C display partly organic character, with an open network structure of mixed $SiC_xN_{(4-x)}$ tetrahedra[38] containing methyl and/or hydrogen terminations. The reduction of hydrogen content from 26 at.% in SiCN-080001 to less than 2.8 at.% in SiCN-120012 is mainly responsible for the pyrolysis shrinkage still observed beyond 800 °C (Fig. 12). While the IR spectra register a decrease in Si–H, Si–CH_3 and C–H band intensities, quantitative information regarding the fractions of the total hydrogen content removed from Si–H and C–H terminations is lacking. However, aggregation of sp^2-carbon into graphitic clusters is detected by Raman analysis in samples thermolyzed above 800 °C. Using simple charge balance considerations, the amount of excess free carbon is estimated from the elemental analysis

data, in the hydrogen free SiCN-120012 and SiCN-130012 samples. Reckoning the invariance of the C/Si and N/Si molar ratios, an equivalent quantity of excess carbon can be expected also in the lower temperature thermolyzed samples, although its organization will depend upon the amount of hydrogen bonded to them. The role of hydrogen depletion in the organization of the polyaromatic carbon in PDC has been reported previously.[35,36] Accordingly, the growth of the graphitic phase proceeds through the stripping of peripheral hydrogen from the H-terminated graphene layers and their subsequent edge-wise association. Recalling the simultaneous increase in the Si–C bond population inferred from IR spectra promoted by the cross-linking reactions involving Si–H, Si–CH_3 and C–H groups, it can be concluded that the progressive hydrogen depletion leads to an increase in the structural density of the thermolyzed materials, through the increased network connectivity of $SiC_xN_{(4-x)}$ units as well as the organization of the graphitic phase. Although the latter process starts as early as by 800 °C pyrolysis, the size of the graphitic domains remain below the critical level in order to be identified as separate phase, up to 1100 °C. Thus, all the samples thermolyzed up to this temperature are amorphous as confirmed by XRD as well as by HRTEM. The phase separation in the material occurs at 1200 °C, beginning with the formation of turbostratic graphite and the nucleation of nano-crystalline SiC at 1300 °C thermolysis.

The effect of the above structural changes is reflected in the physical and mechanical properties of the materials. The increase in the density, elastic modulus and hardness of the materials thermolyzed up to 1000 °C is easily explained in terms of the increased network connectivity realized from the stripping of hydrogen. The change in the elastic and plastic response beyond 1000 °C thermolysis stems from the difference in the nano-structure of the materials. Above this temperature, the size of the graphitic nano-domains reaches a sufficiently high value such that shear deformation is promoted, decreasing the hardness. The growing domains do not immediately degrade the material stiffness, as they remain dispersed as isolated regions in the amorphous network. Interestingly, a recent DFT study of the free carbon in a:Si–C–O materials suggests that the graphitic precipitate bonded to the amorphous network stiffens the structure by decreasing the amount of floppy modes in the structure.[40] In the present case, the increasing modulus of the specimens up to 1200 °C thermolysis coincides with the elimination of hydrogen. At still higher thermolysis temperatures, the growth of the turbostratic graphite phase leads to significant impingement of the layers, as can be partly appreciated from the HRTEM images of the SiCN-130012 sample (Fig. 11c). The decrease in the elastic modulus of the SiCN-130012 specimen is thus attributed to the direct interaction of graphitic precipitates. This is supported by the measured thermal diffusivities of the samples, which show a drastic increase in the SiCN-130012 sample. Electrical conductivity measurements on similar Si–C–N ceramics have displayed an appreciable increase in conductivity, when the growth of turbostratic graphite reached the percolation limit.[41]

From the above discussion, it is evident that the fully dense Si–C–N PDC specimens prepared in this work are suitable for the characterization of their intrinsic mechanical behavior. However, it is to be noted that the structure of the synthesized ceramics are strongly dependant on the processing parameters, viz., cross-linking and pyrolysis temperatures, heating rate, holding time and atmosphere employed. Obviously, the properties of Si–C–N ceramics prepared using different processing parameters can be different. This is also true even for materials which are nominally amorphous as the network density and connectivity of these materials can be different. This effect is illustrated from the comparison of elastic modulus and indentation hardness values of the present materials with those reported by Shah and Raj for a fully dense amorphous Si–C–N ceramic prepared from the PUMVS precursor using a pressure casting route ($E \approx 156$ GPa; $H \approx 26$ GPa; $T_p = 1000$ °C; heating rate: 25 K/h; holding time: 9 h).[20] Nevertheless, investigations using the present materials facilitate to understand the structure–property correlations of typical Si–C–N PDC with respect to their mechanical behavior. A more detailed mechanical characterization of the above materials covering the elastic–plastic deformation and fracture behavior will be presented elsewhere.

5. Conclusions

Fully dense precursor-derived Si–C–N ceramic specimens were fabricated by thermal cross-linking and controlled thermolysis of the PUMVS precursor. Three critical problems were identified and addressed: (a) bubble formation during cross-linking; (b) internal gas pressure induced stress leading to bloating and cracking; (c) stresses from differential transformation due to thermal gradients in the sample. Hydrostatic confinement of the liquid precursor during cross-linking yielded bubble-free glassy green bodies. Pyrolytic stresses were minimized by limiting the green body thickness to 1 mm and by moderating the conductive heat transfer to the sample during thermolysis through a proper choice of the heat transfer media, to produce defect-free dense ceramic bodies.

The range of selected thermolysis treatments enabled the synthesis of ceramic specimens covering material structures from partly organic amorphous to inorganic nano-crystalline states. Structural variation in the amorphous specimens was realized through the stripping of hydrogen with increasing thermal treatment, leading to materials with progressively densified network structures. Phase separated ceramic specimens were obtained from still higher thermolysis treatments. The elimination of hydrogen ensued phase segregation in the material, via the organization of the excess free carbon into a turbostratic graphite phase at 1200 °C and the nucleation of nano-crystalline SiC at 1300 °C thermolysis treatment.

The measured physical and mechanical properties displayed dependency on the material structure. Elastic properties and hardness improved along with the increase in the network density until the onset of phase segregation, where plastic deformation was promoted by the turbostratic graphite phase. Thus, the synthesized specimens are suitable for a detailed mechanical characterization of typical precursor-derived Si–C–N ceramics.

Acknowledgements

The financial support by the Max-Planck-Gesellschaft is gratefully acknowledged. The authors wish to thank Mr. Gerstel and Ms. Müller for useful scientific discussions and Mr. Eckstein, Mr. Kaiser, Mr. Kummer, Mr. Voigt and Mr. Labitzke for the technical support and sample characterization.

References

1. Legrow, G. E., Lim, T. F., Lipowitz, J. and Reaoch, R. S., Ceramics from hydridopolysilazane. *Am. Ceram. Soc. Bull.*, 1987, **66**, 363–367.
2. Chaim, R. and Heuer, A. H., Microstructural and microchemical characterization of silicon-carbide and silicon carbonitride ceramic fibers produced from polymer precursors. *J. Am. Ceram. Soc.*, 1988, **71**, 960–969.
3. Motz, G., Hacker, J. and Ziegler, G., Special modified silazanes for coatings, fibers and CMC's. *Ceram. Eng. Sci. Proc.*, 2000, **21**, 307–314.
4. Motz, G. and Ziegler, G., Simple processibility of precursor-derived SiCN coatings by optimized precursors. *Key Eng. Mater.*, 2002, **206–213**, 475–478.
5. Heimann, D., Bill, J., Aldinger, F., Schanz, P., Gern, F., Krenkel, W. *et al.*, Development of oxidation protected carbon/carbon. *Zeitschrift fuer Flugwissenchaften und Weltraumforschung*, 1995, **19**, 180–188.
6. Wagner, S., Seifert, H. J. and Aldinger, F., High-temperature reactions of C/C–SiC composites with precursor-derived ceramic coatings. *Mater. Manuf. Process.*, 2002, **17**, 619–635.
7. Lee, S. H., Processing of carbon fiber reinforced composites with particulate-filled precursor-derived Si–C–N matrix phases. PhD thesis, Stuttgart: Universität Stuttgart, 2004.
8. Liew, L., Zhang, W., Bright, V. M., An, L., Dunn, M. L. and Raj, R., Fabrication of SiCN ceramic MEMs using injectable polymer-precursor technique. *Sens. Actuators*, 2001, **89**, 64–70.
9. Bill, J. and Aldinger, F., Precursor-derived covalent ceramics. *Adv. Mater.*, 1995, **7**, 775–787.
10. Kroke, E., Li, Y., Konetschny, C., Lecomte, E., Fasel, C. and Riedel, R., Silazane derived ceramics and related materials. *Mater. Sci. Eng. (R)*, 2000, **26**, 97–199.
11. Nishimura, T., Haug, R., Bill, J., Thurn, G. and Aldinger, F., Mechanical and thermal properties of Si–C–N material from polyvinylsilazane. *J. Mater. Sci.*, 1998, **33**, 5237–5241.
12. Galusek, D., Riley, F. L. and Riedel, R., Nanoindentation of a polymer-derived amorphous silicon carbonitride ceramic. *J. Am. Ceram. Soc.*, 2001, **84**, 1164–1166.
13. Bauer, A., Christ, M., Zimmermann, A. and Aldinger, F., Fracture toughness of amorphous precursor-derived ceramics in the silicon–carbon–nitrogen system. *J. Am. Ceram. Soc.*, 2001, **84**, 2203–2207.
14. Seitz, J. and Bill, J., Production of compact polysilazane-derived Si/C/N-ceramics by plastic forming. *J. Mater. Sci. Lett.*, 1996, **15**, 391–393.
15. Konetschny, C., Galusek, D., Reschke, S., Fasel, C. and Riedel, R., Dense silicon carbonitride ceramics by pyrolysis of cross-linked and warm pressed polysilazane powders. *J. Eur. Ceram. Soc.*, 1999, **19**, 2789–2796.
16. Galusek, D., Reschke, S., Konetschny, C. and Riedel, R., Si/C/N amorphous bulk ceramics by axial pressing of polyhydridomethylsilazane at elevated temperature. *Silic. Ind.*, 1998, **63**, 123–128.
17. Wan, J., Gasch, M. J. and Mukherjee, A. K., Silicon carbonitride ceramics produced by pyrolysis of polymer ceramic precursor. *J. Mater. Res.*, 2000, **15**, 1657–1660.
18. Ishihara, S., Gu, H., Bill, J., Aldinger, F. and Wakai, F., Densification of precursor-derived Si–C–N ceramics by high-pressure hot isostatic pressing. *J. Am. Ceram. Soc.*, 2002, **85**, 1706–1712.
19. Freimuth, H., Hessel, V., Kölle, H., Lacher, M., Ehrfeld, W., Vaahs, T. *et al.*, Formation of complex ceramic miniaturized structures by pyrolysis of poly(vinylsilazane). *J. Am. Ceram. Soc.*, 1996, **79**, 1457–1465.
20. Shah, S. and Raj, R., Mechanical properties of a fully dense polymer derived ceramic made by a novel pressure casting process. *Acta Mater.*, 2002, **50**, 4093–4103.
21. Maleki, H., Holland, L. R., Jenkins, G. M., Zimmerman, R. L. and Porter, W., Maximum heating rates for producing undistorted glassy carbon ware determined by wedge-shaped samples. *J. Mater. Res.*, 1996, **11**, 2368–2375.
22. Li, Y., Riedel, R., Steiger, J. and Seggern, H. V., Novel transparent polysilazane glass: synthesis and properties. *Adv. Eng. Mater.*, 2000, **2**, 290–293.
23. Yao, H., Kovenklioglu, S. and Kalyon, D. M., Pore formation in the pyrolysis of polymers to ceramics. *Chem. Eng. Commun.*, 1990, **96**, 155–175.
24. Kalyon, D. M. and Kovenklioglu, S., Processibility of organometallic polymer precursors for non-oxide ceramic applications. *Adv. Polym. Technol.*, 1987, **7**, 191–199.
25. Lewinsohn, C. A., Colombo, P. and Ünal, Ö., Stresses occurring during joining of ceramics using preceramic polymers. *J. Am. Ceram. Soc.*, 2001, **84**, 2240–2244.
26. Sorarù, G. D., Dallapicolla, E. and D'Andrea, G., Mechanical characterization of sol–gel derived silicon oxycarbide glasses. *J. Am. Ceram. Soc.*, 1996, **79**, 2074–2080.
27. Wada, N., Solin, S. A., Wong, J. and Prochazka, S., Raman and IR absorption spectroscopic studies on alpha, beta and amorphous Si_3N_4. *J. Non-Cryst. Solids*, 1981, **43**, 7–15.
28. Janakiraman, N., Weinmann, M., Schuhmacher, J., Müller, K., Bill, J., Aldinger, F. *et al.*, Thermal stability, phase evolution, and crystallization in Si–B–C–N ceramics derived from a polyborosilazane precursor. *J. Am. Ceram. Soc.*, 2002, **85**, 1807–1814.
29. Tuinstra, F. and Koenig, J. L., Raman spectrum of graphite. *J. Chem. Phys.*, 1970, **53**, 1126–1130.
30. Ferrari, A. C. and Robertson, Resonant Raman spectroscopy of disordered, amorphous, and diamondlike carbon. *J. Phys. Rev. B*, 2001, **64**, 075414.
31. Ferrari, A. C. and Robertson, Interpretation of Raman spectra of disordered and amorphous carbon. *J. Phys. Rev. B*, 2000, **61**, 14095–14107.
32. Nemanich, R. J. and Solin, S. A., 1st-order and 2nd-order Raman-scattering from finite-size crystals of graphite. *Phys. Rev. B*, 1979, **20**, 392–401.
33. Wang, Y., Alsmeyer, D. C. and McCreery, R. L., Raman-spectroscopy of carbon materials—structural basis of observed spectra. *Chem. Mater.*, 1990, **2**, 557–563.
34. Haug, J., Untersuchung der Struktur und des Kristallisationsverhaltens von Si–C–N– und Si–B–C–N–Precursorkeramiken mit Röntgen und Neutronenbeugung. PhD thesis, Stuttgart: Universität Stuttgart, 2002.
35. Monthioux, M. and Delverdier, O., Thermal behavior of (organosilicon) polymer-derived ceramics 5. Main facts and trends. *J. Eur. Ceram. Soc.*, 1996, **16**, 721–737.
36. Gregori, G., Kleebe, H. J., Brequel, H., Enzo, S. and Ziegler, G., Microstructure evolution of precursors-derived SiCN ceramics upon thermal treatment between 1000 and 1400 °C. *J. Non-Cryst. Solids*, 2005, **351**, 1393–1402.
37. Turquat, C., Kleebe, H. J., Gregori, G., Walter, S. and Soraru, G. D., Transmission electron microscopy and electron energy-loss spectroscopy study of nonstoichiometric silicon–carbon–oxygen glasses. *J. Am. Ceram. Soc.*, 2001, **84**, 2189–2196.
38. Li, Y., Kroke, E., Riedel, R., Fasel, C., Gervais, C. and Babonneau, F., Thermal cross-linking and pyrolytic conversion of poly(ureamethylvinyl)silazanes to silicon-based ceramics. *Appl. Organometall. Chem.*, 2001, **15**, 820–832.
39. Bauer, A., Einfluss der Herstellungsparameter auf die mechanischen Eigenschaften von Si–(B–)C–N–Precursorkeramiken. PhD thesis, Stuttgart: Universität Stuttgart, 2002.
40. Kroll, P., Modeling the 'free carbon' phase in amorphous silicon oxycarbide. *J. Non-Cryst. Solids*, 2005, **351**, 1121–1126.
41. Trassl, S., Puchinger, M., Rössler, E. and Ziegler, G., Electrical properties of amorphous $SiC_xN_yH_z$-ceramics derived from polyvinylsilazane. *J. Eur. Ceram. Soc.*, 2003, **23**, 781–789.